JOURNAL OF CHEMICAL INFORMATION AND MODELING

ARTICLE

pubs.acs.org/jcim

New Aryl Hydrocarbon Receptor Homology Model Targeted To Improve Docking Reliability

Ilaria Motto,[§] Annalisa Bordogna,[§] Anatoly A. Soshilov,[#] Michael S. Denison,[#] and Laura Bonati*[,§]

[§]Dipartimento di Scienze dell'Ambiente e del Territorio, Università degli Studi di Milano-Bicocca, Piazza della Scienza 1, 20126 Milano, Italy

[#]Department of Environmental Toxicology, Meyer Hall, University of California, Davis, California 95616, United States

Supporting Information

ABSTRACT: The aryl hydrocarbon receptor (AhR) is a ligand-dependent, basic helix−loop−helix Per-ARNT-Sim (PAS) containing transcription factor that can bind and be activated by structurally diverse chemicals, including the toxic environmental contaminant 2,3,7,8-tetrachlorodibenzo-p-dioxin (TCDD). As no experimentally determined structures of the AhR ligand binding domain (LBD) are available and previous homology models were only derived from *apo* template structures, we developed a new model based on *holo* X-ray structures of the hypoxia-inducible factor 2α (HIF-2α) PAS B domain, targeted to improve the accuracy of the binding site for molecular docking applications. We experimentally confirmed the ability of two HIF-2α crystallographic ligands to bind to the mAhR with relatively high affinity and demonstrated that they are AhR agonists, thus justifying the use of the *holo* HIF-2α structures as templates. A specific modeling/docking approach was proposed to predict the binding modes of AhR ligands in the modeled LBD. It was validated by comparison of the calculated and the experimental binding affinities of active THS ligands and TCDD for the mAhR and by functional activity analysis using several mAhR mutants generated on the basis of the modeling results. Finally the ability of the proposed approach to reproduce the different affinities of TCDD for AhRs of different species was confirmed, and a first test of its reliability in virtual screening is carried out by analyzing the correlation between the calculated and experimental binding affinities of a set of 14 PCDDs.

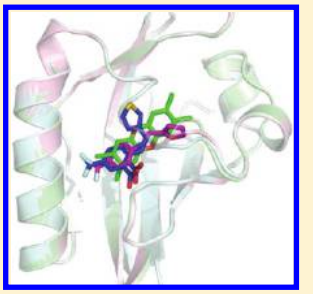

INTRODUCTION

The aryl hydrocarbon receptor (AhR) is a basic helix−loop−helix (bHLH), Per-ARNT-Sim (PAS) containing ligand-dependent transcription factor that induces the expression of a large battery of genes and produces diverse biological and toxic effects in a wide range of species and tissues.[1−4] The best-characterized high affinity ligands include a variety of toxic halogenated aromatic hydrocarbons (HAHs), such as the polychlorinated dibenzo-p-dioxins (PCDDs), dibenzofurans (PCDFs), and biphenyls (PCBs), and numerous polycyclic aromatic hydrocarbons (PAHs) and PAH-like chemicals,[5−7] all widespread classes of environmental contaminants. Moreover, a number of natural, endogenous, and synthetic AhR agonists and antagonists whose structure and physicochemical characteristics are different from those of the prototypical HAH and PAH ligands have been identified as lower affinity ligands and moderately potent inducers of AhR-dependent gene expression.[7−11] Among the various protein domains responsible for the AhR functional activities, PAS B (one of the two structural repeats in the PAS domain) is the one responsible for ligand binding, and it is also involved in binding to the chaperone heat shock protein 90 (hsp90).[12]

Although the AhR signal transduction pathway has been studied for many years,[1−4] several unanswered questions remain. Major issues are the actual spectrum of ligands, how they can bind to the AhR, and how ligand binding to the ligand binding domain (LBD) results in activation of the AhR and AhR-dependent gene expression. A molecular understanding of these events would require detailed structural information about the AhR PAS B LBD. However, neither X-ray nor NMR structures of the bound or unbound AhR have been determined to date.

Since the first crystal structures of distant homologous proteins belonging to the PAS superfamily became available, we started developing theoretical models of the AhR LBD by homology modeling techniques and the results provided an initial framework to make hypotheses on LBD characteristics and the mechanisms of AhR functionality.[9,13,14] The latest model of the mouse AhR (mAhR) LBD we proposed[14] was built using the NMR structures of the PAS B domains of the human hypoxia-inducible factor 2α (HIF-2α)[15] and of the human ARNT,[16] both in the *apo* form, as templates. That was the most reliable among the models developed in our group, since the template domains show the highest degree of sequence identity and similarity with the AhR PAS B among all the PAS structures reported to date. Moreover, the full length template proteins are members of the bHLH/PAS family of transcriptional factors and functionally related to the AhR.[4] On the basis of model-driven site-directed mutagenesis and AhR functional analysis, the buried cavity in the core of the domain was confirmed as the site involved in ligand

Received: April 11, 2011
Published: October 09, 2011

binding.[14] Moreover, analysis of the LBD models of several mammalian AhRs indicated that the physicochemical characteristics of the binding cavities are remarkably conserved in all AhRs with high affinity for the AhR ligand 2,3,7,8-tetrachlorodibenzo-p-dioxin (TCDD).[17] Mutagenesis of the conserved residues, followed by AhR functional analysis, allowed identification of the "TCDD-binding fingerprint", i.e. the group of residues necessary for optimal TCDD binding.[17]

On the basis of our findings, other authors recently reported the development of AhR LBD homology models based on the same *apo* structure of HIF-2α and proposed the use of these models for molecular docking applications.[18−22] Although the use of homology models of the target protein, in addition to experimental structures, has greatly extended the applicability of molecular docking approaches,[23−25] the use of good quality models, in particular of the binding site, is crucial for the prediction of reliable binding poses.[24,26−28] In fact, it was proven that the success of docking calculation decreases with the quality of the receptor structure and, in particular, with the decreasing ability of the structure to reproduce the features of the active site that are important for ligand recognition. Modeled structures, even those having high sequence identity to their template structure, can have improperly placed side chains in the binding site. This can be partially overcome by the use of *holo* template structures, that take into account the induced fit effects associated with the presence of a ligand in the binding cavity, thus greatly improving the quality of the modeled cavity and the reliability of the predicted binding modes of similar ligands.[26,29] Since all of the AhR LBD models developed to date were derived from *apo* template structures, their use in molecular docking could have some limitations.

The recent depositions of new X-ray structures of the human HIF-2α:ARNT PAS B heterodimer cocrystallized with artificial ligands[30,31] provided us with an opportunity to improve the quality of the modeled AhR binding site. With their studies, Gardner and co-workers demonstrated that other PAS domains, in addition to the AhR, are able to bind small-molecule ligands.[30−32] Moreover, they highlighted that the crystal structures of the ligand-bound HIF-2α PAS B domain show larger binding cavities and have important conformational differences compared to the *apo* structures previously determined by NMR.[30,31]

Demonstration of the ability of these HIF-2α ligands to bind to the AhR LBD would suggest similarities in features of the two binding cavities that are involved in ligand recognition. This experimental finding would also justify the use of the new ligand-bound HIF-2α three-dimensional structures to develop a new homology model of the AhR LBD, specifically targeted to improve the accuracy of the binding site for molecular docking applications aimed to reliably analyze the binding modes of the wide spectrum of chemicals that bind to the AhR.

Here we demonstrate the binding and agonist activity of HIF-2α crystallographic ligands[30,31] to the AhR, confirming the choice of using the above-mentioned ligand-bound HIF-2α complexes as templates for the AhR LBD modeling. Using this improved model, we propose to predict the binding modes of AhR ligands in the modeled LBD by a specifically developed docking approach. First, validation of the homology modeling/docking approach is performed by comparison of the calculated and the experimental binding affinities of active THS ligands and TCDD for the mAhR. Moreover, the predicted TCDD binding mode within the binding cavity is confirmed by functional activity analysis using several mAhR mutants generated on the basis of the modeling results. Ligand binding to new homology models of the human AhR (huAhR) and the rat AhR (rtAhR) is also analyzed. With this information, the ability of the proposed approach to reproduce the different affinities of TCDD for AhRs of different species[33] was verified and a first test of its reliability in virtual screening applications is carried out by analyzing the correlation between the calculated and experimental binding affinities of a set of 14 PCDDs for the rtAhR.[34,35]

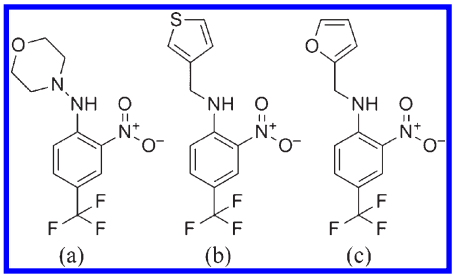

Figure 1. THS compounds used in these studies. The structure of (a) THS-044, (b) THS-017, (c) THS-020.

RESULTS AND DISCUSSION

THS Ligands Can Bind to and Activate the mAhR LBD. A series of synthetic compounds that could bind to and be cocrystallized with a recombinant HIF-2α PAS B fragment[31] has recently been reported. Considering that both HIF-2α and AhR proteins belong to the same superfamily and have PAS B domains with relatively high sequence identity and similarity, we hypothesized that these compounds might also bind to the AhR. Accordingly, we examined the ability of three of these compounds (THS-017, THS-020, and THS-044 (Figure 1)) to compete with [^{3}H]TCDD for binding to *in vitro* synthesized mAhR.[36] Preliminary experiments demonstrated that THS-017 and THS-020, but not THS-044, could competitively inhibit the specific binding of [^{3}H]TCDD to the AhR (data not shown). Accordingly, to estimate the relative ligand binding affinity of these new AhR ligands, competitive hydroxyapatite binding assays with *in vitro* synthesized mAhR were carried out with 2 nM [^{3}H]TCDD in the absence or presence of increasing concentrations of THS-017 and THS-020.[36] These experiments revealed that THS-017 and THS-020 could competitively displace [^{3}H]TCDD specific binding to the AhR in a concentration-dependent manner (Figure 2A). Relative binding affinity values (IC_{50}) for THS-017 ($\sim$0.6 μM) and THS-020 ($\sim$4.2 μM) were determined by nonlinear regression analysis of the competitive binding curves and demonstrate that these ligands have significantly lower affinity than that of TCDD (1 nM).[37,38] While binding analysis confirms the ability of the compounds to directly interact with the AhR, it does not provide any information as to the functional activity of the ligand. To determine whether these ligands were AhR agonists, we examined their ability to stimulate DNA binding of *in vitro* synthesized mAhR (using gel retardation analysis) and AhR-dependent gene expression in cells in culture (using transient transfection). Both THS-017 and THS-020 could stimulate mAhR DNA binding in a concentration-dependent manner (Figure 2B), and the amount of induced THS-017/THS-020:AhR:ARNT:DNA complex formed at each concentration from multiple experiments was determined and expressed relative to that produced by a maximal activating concentration of TCDD

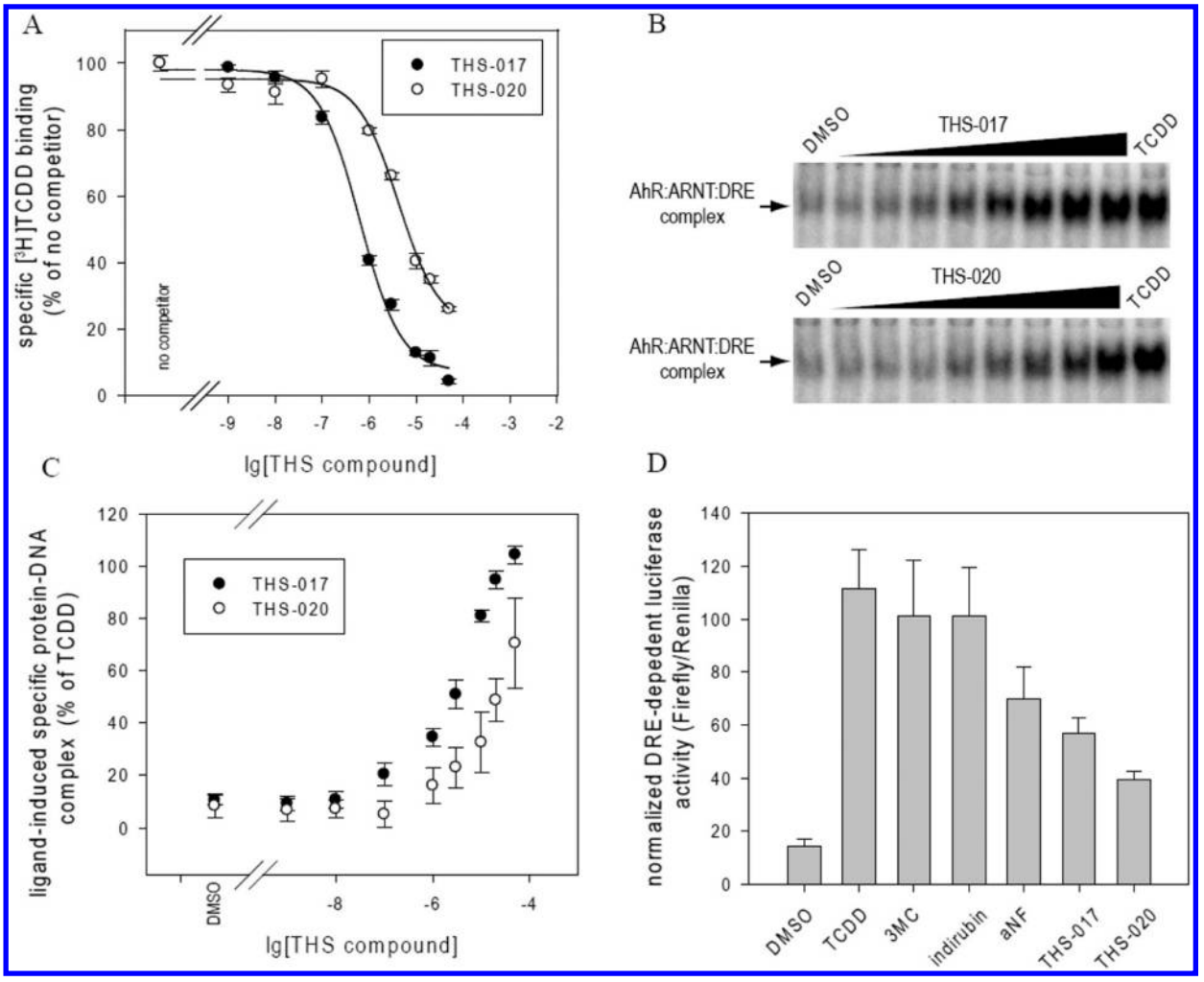

Figure 2. THS-017 and THS-020 bind to and activate the AhR. A. THS compounds displace [^{3}H]TCDD from the *in vitro* synthesized AhR in concentration-dependent manner. *In vitro* synthesized AhR was diluted in MEDG buffer at 8:92 ratio and incubated with 2 nM [^{3}H]TCDD and increasing concentrations of THS-017 or THS-020 for 30 min at room temperature. Ligand binding was measured by the hydroxyapatite assay. Values are presented as the means ± standard deviations of three independent experiments. The resulting IC50 values from these competitive curves were 0.6 μM for THS-017 and 4.2 μM for THS-020. B, C. THS compounds stimulate AhR DNA binding. *In vitro* synthesized AhR and ARNT were diluted in MEDGK buffer (MEDG supplemented with 0.15 M KCl) at 1.5:1.5:7 ratio and incubated in the presence of 10 nM TCDD or increasing concentrations of THS compounds (or 1% v/v DMSO) for 2.5 h at room temperature, and DNA binding by activated AhR:ARNT complex was analyzed by gel retardation assay. Gels were visualized with FLA9000 (Fujifilm). C. Specific bands were quantitated in MultiGauge (Fujifilm). Values are presented as the means ± standard deviations of three independent experiments. D. THS compounds activate AhR-dependent gene expression. COS-1 cells were transiently transfected with the AhR expression vector, AhR-dependent firefly luciferase reporter, and Renilla luciferase internal control. In 24 h post transfection, cells were treated with 0.1% (v/v) DMSO, 10 nM TCDD, 1 μM 3MC or indirubin, 10 μM aNF, or 20 μM THS-017 or THS-020 for 24 h, lyzed, and analyzed for dual luciferase reporter activity. Values are presented as the means ± standard deviations of three independent experiments. All compounds activated reporter gene expression at values that were statistically higher than that of DMSO (solvent control) at $P < 0.05$ as determined by the Student's *t* test. A-D. Results are representative of two or three independent experiments.

(Figure 2C). The relative binding affinity of THS-017 and THS-020 (Figure 2A) compares favorably with the relative potency of each to stimulate mAhR DNA binding (Figure 2B/C), with THS-017 having a slightly greater affinity and potency. The ability of these compounds to stimulate AhR transformation and DNA binding is consistent with their ability to act as AhR agonists. To confirm this, we examined the ability of THS-017 and THS-020 to stimulate AhR-dependent luciferase reporter gene expression. COS-1 cells that had been transiently cotransfected with a mAhR expression vector and an AhR-responsive luciferase plasmid (pGudLuc6.1)[39] were incubated for 24 h with THS-017, THS-020, or several known AhR agonists (TCDD, 3-methylcholanthrene (3MC), indirubin, or alpha-naphthoflavone (aNF)) and luciferase activity determined. These results clearly demonstrate the ability of both THS-017 and THS-020 to stimulate AhR-dependent gene expression and although they were less potent than the well established AhR agonists TCDD, 3MC, and indirubin, they were comparable to the lesser potent AhR agonist aNF. Together, these results demonstrate that THS-017 and THS-020 are AhR agonists with affinities and potencies comparable to many well-characterized AhR ligands,[40] and they provide strong justification for use of the crystal structures of THS-bound HIF-2α as improved templates for modeling the AhR LBD.

Table 1. PDB Structural Information Available on HIF-2α/THS Ligand Complexes

PDB ID	chain	resolution (Å)	missing residues	ligand name
3F1O	A	1.60	329−333	THS-044
3H7W	A	1.65	328−333	THS-017
3H82	A	1.50	none	THS-020

mAhR Homology Modeling. Homology modeling techniques were applied to predict the LBD structure (residues 278−384) of the mAhR that takes into account the presence of ligands in its binding site. In fact, an improved description of the binding cavity in the bound form makes the mAhR model more suitable for accurate docking calculations and virtual screening applications[26] than the models based on previously proposed *apo* template structures.[14,17] This new homology model was derived by monotemplate sequence alignment with the HIF-2α PAS B domain, for which multistructural information exists. The availability of experimental structures of the HIF-2α PAS B domain cocrystallized with THS ligands (PDB ID: 3F1O,[30] 3H7W,[31] 3H82[31]) provides optimal template structures to improve the AhR PAS B homology model for docking applications. Their properties are summarized in Table 1. Although our experiments demonstrated that only THS-017 and THS-020 act as AhR agonists, all three template structures were used in the homology modeling. In fact, while the ligand binding site is highly conserved among the three crystallized THS:HIF-2α PAS B, the combined use of the three structures does provide a better statistical representation of the possible conformational variability of the whole protein in the bound form.

The sequence alignment of the mAhR and the HIF-2α template previously proposed[14,17] was employed for modeling. Analysis of the alignment (Figure SI1) demonstrates that the major part of the AhR LBD can be modeled on the basis of all the three X-ray depositions of the template. A short region, corresponding to the Hβ/Iβ loop (the secondary structures attributed by DSSPcont[41] are shown in the figure), is solved only in one template structure (PDB ID: 3H82).

The crystallographic structures of the three templates were prepared as described in the Experimental Section. One-hundred three-dimensional models for the mAhR LBD were generated using MODELLER[42−45] and energetically ranked by the DOPE score[46] (see Experimental Section). The template-bound structures of the THS ligands (Figure 1) were transferred into the mAhR homology models for the purpose of obtaining a binding cavity that takes into account ligand induced-fit effects.

The first visual inspection of the resulting one-hundred mAhR homology models highlighted some conformational variability in the Hβ/Iβ loop and around the inserted Gly 313 (Figure SI2). The flexibility of the Hβ/Iβ loop can be ignored as it does not influence the dimension of the binding site. In contrast, the conformational variability observed around Gly 313, that lines the ligand binding cavity, was further analyzed since the dynamic behavior of the binding site must be taken into account for docking applications. Based on these observations, a workflow for the selection of representative conformations of the mAhR binding site was established, and the implemented selection funnel is presented in Scheme 1.

Five conformational clusters for the AhR were identified, and the almost regular membership distribution in clusters 1−4 confirmed a dynamic binding site behavior. Since only two conformers populate cluster 5, it can be considered statistically less representative in the description of the mAhR conformational variability, and thus it was not included in subsequent modeling analyses and applications.

Scheme 1. Workflow for the Selection of mAhR Representative Binding Site Conformations

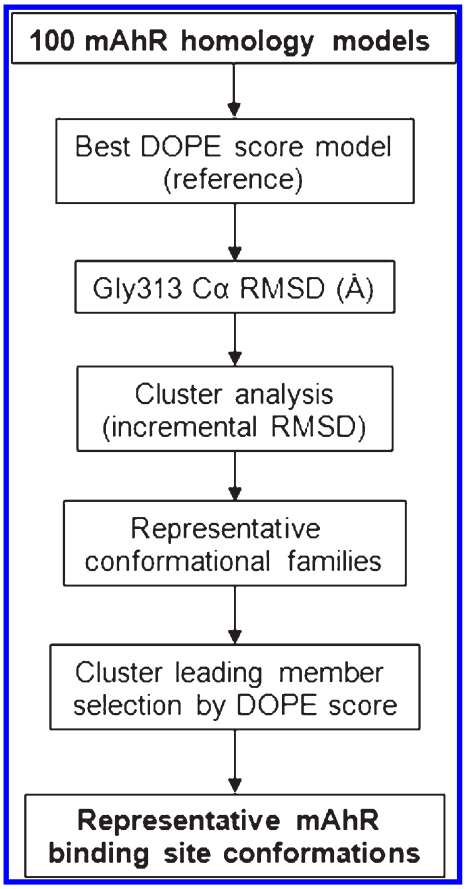

PROCHECK[47] validation of the selected representative conformations of each cluster indicated a good stereochemical quality, with 87−91% of residues belonging to the most favored areas of the Ramachandran plot and overall G-factors ranging from −0.26 to −0.19 (this index ranges from −0.5 to 0.3 for structures solved at 1.5 Å resolution). Moreover the ProSA z-scores[48,49] values were between −4.14 and −3.87, within the range of values typical for native protein structures of similar size.

Comparison of the *apo* and *holo* Homology Models. Comparative analysis of the new mAhR homology models (*holo* mAhR) and the previously published model (*apo* mAhR[14,17]) was carried out to elucidate the effects of using *holo* template structures and including ligands during the binding site modeling. The global and the binding site rmsd of the *holo* mAhR representative conformations (in the following also named representative homology models, HM) were calculated relative to the *apo* mAhR model. The resulting values (Table 2) revealed that significant contributions to the global rmsd appear to derive from differences in the conformations of the binding site residues. Focusing on the comparative analysis of residues within 5 Å of the THS ligands in the *holo* model, several important differences between the *apo* and *holo* AhR LBD models appear. Particularly evident is the different conformation of the His 320 residue, whose side chain is projected into the binding site in the

Table 2. RMSD between the mAhR *apo* and the Representative *holo* Homology Models (HM01, HM70, HM77, and HM79)

	global rmsd (Å)			binding site[a] rmsd (Å)			TCDD-binding fingerprint[b] rmsd (Å)		
mAhR	total	backbone	side chain	total	backbone	side chain	total	backbone	side chain
HM01	2.27	1.43	2.86	5.93	3.63	5.76	2.01	1.31	2.42
HM70	2.3	1.32	2.96	5.69	3.60	5.51	1.90	1.31	2.26
HM77	2.37	1.43	3.01	5.75	3.63	5.76	2.19	1.30	2.70
HM79	2.29	1.34	2.93	5.63	3.62	5.66	2.00	1.31	2.40

[a] Residues in a 5 Å shell around the THS ligands are considered to define the binding site. [b] The group of residues necessary for optimal TCDD binding as determined by mutagenesis and functional analysis[17] is considered.

Table 3. Connolly Accessible Volumes of the Main Cavity for the HIF-2α Templates, the *apo* mAhR Model, and the Representative *holo* mAhR Models (HM01, HM70, HM77, and HM79) Calculated by the CASTp Web Server

HIF-2α templates	
structure	Connolly accessible volume (Å^3)
1P97 (NMR conf. 17, *apo*)	123
3F1O (X-ray, *holo*)	424
3H7W (X-ray, *holo*)	421
3H82 (X-ray, *holo*)	439
mAhR homology models	
homology model	Connolly accessible volume (Å^3)
mAhR (*apo*)	471
HM01 (*holo*)	813
HM70 (*holo*)	887
HM77 (*holo*)	790
HM79 (*holo*)	845

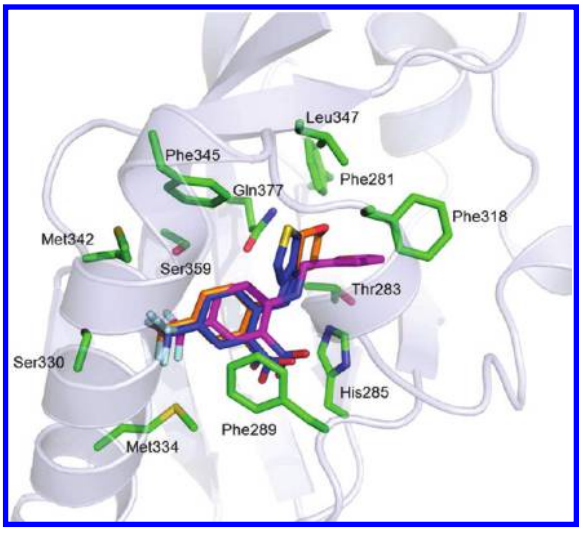

Figure 3. Post-energy minimization conformations of the mAhR_HM79+THS-017 (blue), mAhR_HM70+THS-020 (magenta), and mAh_HMR01+THS-044 (orange) complexes. The most interesting interacting residues are shown as sticks. Secondary structures were attributed by DSSPcont.[41]

apo model while it is projected outside in the *holo* models. This directly results from the different structural depositions used in the homology modeling. In fact, in the sequence alignment (Figure SI1), AhR His 320 corresponds to His 282 in HIF-2α and it points away from the binding site in the utilized templates, while in the NMR *apo* HIF-2α structure (PDB ID: 1P97[15]), used in the previous homology modeling studies,[14,17] His 282 points inward. However, it is conceivable that this conformational effect is not related to a structural rearrangement of the binding site that occurs upon ligand binding but to crystallographic packing, since His 282 adopts the same outward conformation in all the available X-ray structures of HIF-2α, including the *apo* ones.[30,31] Other conformational differences between the *apo* and *holo* template structures (i.e., side chain and backbone shifts) are also observed for residues lining the binding pocket, and they are clearly reflected in the respective mAhR homology models. In fact, the rmsd values between the residues identified as the "TCDD-binding fingerprint"[17] in the *holo* and in the *apo* mAhR models (Table 2) indicate that significant conformational changes were induced in these side chains by the use of *holo* template structures.

Since the internal cavity volume is determined by the conformations assumed by the internal binding site residues, the CASTp[50] Web server[51] was used to calculate and compare the accessible Connolly's volumes[52] for the main cavity of the HIF-2α templates, the published *apo* and the representative *holo* mAhR homology models. The results in Table 3 indicate a clear ligand induced-fit effect on the binding site extension, with inclusion of THS ligands in mAhR binding site almost doubling the cavity volume. Comparison of selected *holo* mAhR homology models with the HIF-2α templates reveals a more extended "channel-like" binding cavity. Superimposition of these models with the templates shows an outward shift of the Aβ strand that could explain the observed longer extension of the mAhR ligand binding site.

Evaluation of the THS Ligands Binding Mode in mAhR. THS compounds were rigidly copied from the HIF-2α structural templates into the mAhR binding site during the homology modeling process. The representative conformations complexed with the HIF-2α ligands were subjected to energy minimization as described in the Experimental Section. This permitted relaxation of THS ligands in their new protein environment, in order to facilitate the evaluation of their possible binding mode in the mAhR LBD.

All the energy minimized complexes were ranked using Glide extra precision (XP) scoring function,[53] and the representative complexes with the best scores (mAhR_HM79+THS-017, mAhR_HM70+THS-020, and mAhR_HM01+THS-044) were chosen for more focused structural analysis. An intramolecular hydrogen bond between the ligand aniline and nitro group, similar to the one described for the crystallographic HIF-2α/THS complexes,[30,31] was

Table 4. Calculated Pre-/Post-energy Minimization RMSD for the THS Ligands in the Representative *holo* mAhR Homology Models (HM01, HM70, HM77, and HM79)

mAhR	THS-017 rmsd (Å)	THS-020 rmsd (Å)	THS-044 rmsd (Å)
HM01	1.77	1.05	0.82
HM70	1.70	1.93	1.25
HM77	1.10	1.12	1.42
HM79	1.42	0.80	1.13

observed also in the minimized complexes (Figure 3). This bond provides a high internal stabilization and favors a stable bent conformation of the ligands. Polar interactions of the amino and nitro groups with the His 285 and the Gln377 side chains anchor the central part of the ligand molecules. The trifluoromethyl group, that lies at the entrance of the cavity in a hydrophobic environment, is also subjected to some stabilizing polar interactions with Ser 330 and Ser 359, whereas the aryl ring is packed with the side chains of Phe 289 and Phe 345. As highlighted above, the mAhR LBD shows a more extended binding cavity than HIF-2α. Given the low calculated rmsd between the ligand structures pre- and post-energy minimization (Table 4), the binding conformations of the THS ligands appear almost conserved after the energy minimization. However, as both THS-017 and THS-020 contain a flexible spacer (methylene group), they can assume slightly more extended conformations in mAhR than in HIF-2α by projecting their heterocyclic rings deeper into the mAhR cavity, in a highly hydrophobic region. As shown in Figure 3, the chemical properties and the binding conformations observed for the heterocycles of THS-017, THS-020, and THS-044 in this zone seem to correlate with the relative order of their experimental affinities. In fact, the thiophene ring in THS-017 is highly hydrophobic and thus would be particularly well stabilized in this environment by favorable van der Waals contacts. The furan group in THS-020 would also prefer hydrophobic surroundings, but the harder oxygen atom introduces some system polarity; in the derived model only the side chains of Thr 283, His 285, and Gln 377 could help in stabilizing this slightly polar system. In contrast, the placement of the polar and basic morpholine group of THS-044 would not be favored in this binding site area, and this destabilization could explain its extremely low affinity for the AhR compared to the other THS ligands. Considering the experimental affinity data we obtained for the THS compounds in mAhR, THS-044, that does not bind mAhR, was excluded from further modeling investigations.

Ensemble Docking Approach To Study Ligand Binding to the AhR. As discussed above, in mAhR homology models some conformational variability is observed around Gly 313. This residue and its surroundings line the ligand binding pocket, and its dynamic behavior could influence the dimensions of the cavity and consequently ligand placement. For this reason, its dynamics should be taken into account during docking calculations. However, incorporating protein flexibility during molecular docking still remains one of the major challenges of this method.[54,55] Although numerous programs allow induced-fit docking, these calculations still remain computationally expensive, time-consuming, and not suitable for virtual screening. Accordingly, ensemble docking[56] was selected as the optimal approach to perform the "dynamic" docking of ligands in the mAhR homology model, using the representative homology models selected by cluster analysis to describe discrete conformational states of the binding site in which ligands could explore different binding modes. The Glide program was used to perform an exploratory ligand docking, and, in order to establish a general approach, we selected the Glide standard precision (SP) protocol.[57−59] The described approach was initially applied for the redocking of the two THS ligands that bind the mAhR, in order to test its ability in reproducing the reference binding modes derived from the HIF-2α templates and relaxed in the mAhR binding site (Figure 3). The starting conformation of each THS ligand is the global minimum conformer (obtained as described in the Experimental Section); in both cases it belongs to the same conformational cluster of the crystallographic structure. To broadly explore the conformational variability of the flexible THS ligands, the first 10 docking poses for each representative mAhR conformation were analyzed. Two clusters of poses were obtained for both ligands, and the most populated cluster (60% for THS-017, 73% for the THS-020) reproduces the reference binding mode. The pose with the lowest rmsd to the reference obtained in each representative mAhR conformation was retained and subjected to energy minimization, according to the protocol described in the Experimental Section. Finally, the energy minimized complexes were ranked on the basis of the rmsd to the reference. The best final poses (Figure SI3) reproduce well the ones obtained from the templates, with global rmsd values of 2.74 Å, for the THS-017, and 0.43 Å, for THS-020. Only a conformational rearrangement of the THS-017 thiophene ring, due to the flexibility of the connecting methylene group, is observed. The network of stabilizing interactions with the mAhR previously discussed (Figure 3) was maintained in these poses.

TCDD is the highest affinity and most potent AhR ligand.[6,40] Considering its extremely high potency and toxicity in many species, it has been widely studied in order to assess the structural determinants that drive its strong association with the AhR. The TCDD best-ranked docking poses in the representative mAhR conformations, obtained applying our docking protocol, are shown in Figure 4a. Three clusters of TCDD placements within the cavity are observed: an "internal" pose (in mAhR_HM01), two "central" poses (in mAhR_HM70 and mAhR_HM77), and an "external" pose (in mAhR_HM79). Energy minimization of the complexes (see the Experimental Section) permitted the relaxation of the TCDD molecule, its 5 Å shell of surrounding residues, and the residues that we experimentally identified as the TCDD binding fingerprint (Thr 283, His 285, Phe 289, Tyr 316, Ile 319, Phe 345, and Ala 375).[17] After the energy minimization, almost all the docking poses converge in one conformational cluster that occupies the middle of the cavity, suggesting a favorable intermolecular interaction network in this zone.

To better investigate the observed positional convergence of TCDD in the representative mAhR homology models, we carried out combined Monte Carlo/Stochastic Dynamics (MC/SD) simulations.[60] The MC/SD procedure differs from a normal dynamics simulation in that it uses a mixture of Metropolis Monte Carlo[61] and dynamics steps in order to greatly increase the rate at which a simulation explores conformational space. The "internal" (mAhR_HM01+TCDD) and "external" (mAhR_HM79+TCDD) poses obtained by molecular docking were selected as starting conformations for 1.5 ns of MC/SD simulations. These simulations revealed that TCDD could move within the cavity by 0.4−4.0 Å of the rmsd, relative to its starting conformations. Almost 30% of the TCDD conformational population sampled during the MC/SD showed a hydrogen bond with the Thr 283 side chain and almost 70% forms a hydrogen bond with the Gln 377 side chain, thus

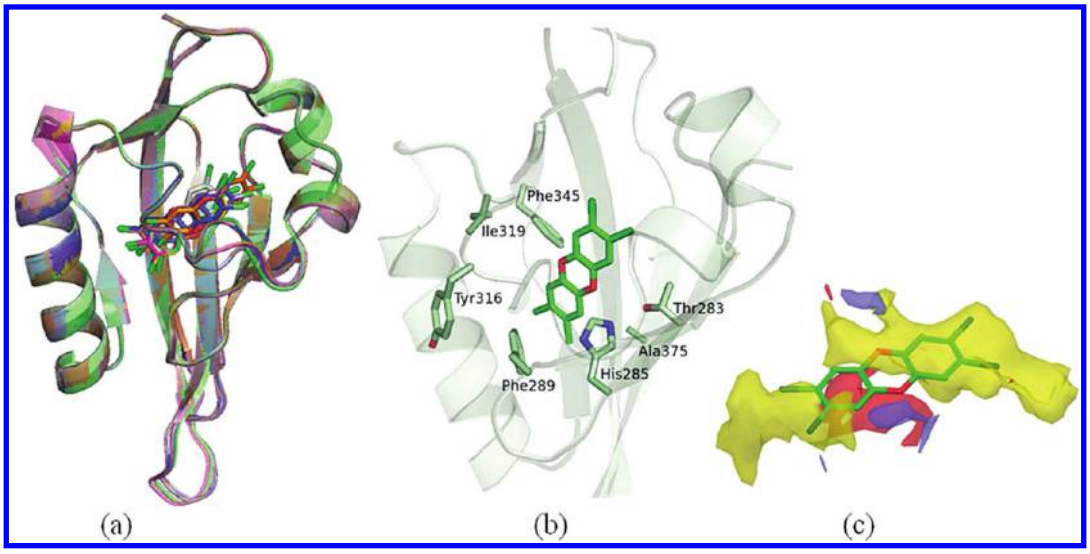

Figure 4. TCDD ensemble docking in mAhR homology models (HM01+TCDD: green, HM70+TCDD: magenta, HM77+TCDD: yellow, HM79+TCDD: blue): (a) Glide SP docking poses and (b) Glide XP best scoring post-energy minimization complex (HM01+TCDD, green). The fingerprint residues for TCDD[17] are shown as stick. (c) mAhR binding site mapping (yellow: hydrophobic site at −0.5 kcal/mol; blue: hydrogen bond donor site at −8 kcal/mol; red: hydrogen bond acceptor site at −8 kcal/mol). Glide XP best scoring pose for TCDD is shown.

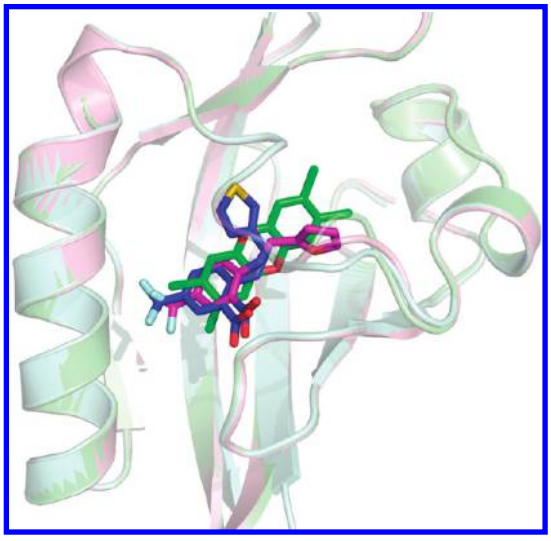

Figure 5. Superimposition of the Glide XP best scoring docking pose of the TCDD (HM01+TCDD: green) and the binding modes derived from the HIF-2α templates for the THS-017 (HM79+THS-017: blue) and THS-020 (HM70+THS-020: magenta).

confirming a certain degree of stabilization of the ligand in the middle part of the cavity. MC/SD results appear to correlate with both the observed docking poses and the energy minimization results and indicate that TCDD, a highly symmetric and flat molecule, can explore the cavity extension but seems better stabilized within the middle of the binding site where its oxygen atoms can form hydrogen bonds with Thr 283 and Gln 377 side chains.

The energy minimized mAhR/TCDD complexes were ranked using Glide extra precision (XP) scoring function[53] in order to select a representative complex. The best scoring complex (mAhR_HM01+TCDD) is shown in Figure 4b. The mAhR binding site was mapped using SiteMap program[62] in order to verify matching between the ligand and protein properties. An

Table 5. Glide XP Best Scoring Complexes for the *holo* mAhR Models Bound to TCDD and the THS Ligands, Compared to the Experimental Relative Affinity (IC_{50}) Values Obtained with *in Vitro* Synthesized mAhR

	Glide XP score		
Ligand	Complex derived from the templates	Complex obtained by docking	Experimental IC_{50} (M), *in vitro* synthesized mAhR
TCDD		−8.70	1×10^{-9} [a]
THS-017	−6.71	−6.78	0.63×10^{-6}
THS-020	−6.56	−6.68	4.2×10^{-6}

[a] C57 mAhR TCDD binding affinity.[37,38]

extended hydrophobic channel was identified at −0.5 kcal/mol together with smaller hydrogen bond donor and acceptor globular volumes at −8 kcal/mol. TCDD fills the hydrophobic channel and orients one oxygen atom near the hydrogen bond acceptor spot (Figure 4c). Thus, the observed ligand binding placement seems to satisfy the mAhR physicochemical requirements. Superimposition of the best scored complexes for TCDD and the THS ligands allowed direct comparison of the binding mode for all the ligands (Figure 5). TCDD and the THS ligands occupy almost the same region in the binding site. However TCDD is projected slightly more into the cavity than the THS ligands. In fact the former is a rigid and flat molecule, while the latter ligands assume a stable bent conformation driven by the intramolecular hydrogen bond between the amino and nitro groups.

Computational and Experimental Data Correlation Analysis. The Glide XP scores for the best mAhR/ligand complexes, both obtained by docking and derived from the templates, are summarized in Table 5. In both cases, the computational ranking is coherent with the differences observed in the experimental ligand binding affinities between the TCDD and the THS ligands. However, the scoring function applied is not sensitive

Table 6. Effects of mAhR Mutagenesis on TCDD Binding[d]

	effect of indicated mutation on TCDD binding		
residue	reduced to less than 50%	reduced to 50−60%	little or no effect
F281			F281W[b]
T283[a]	T283E, T283M		
H285[a]	H285F, H285A		
F289[a]	F289A, F289L, F289Y		
P291	P291F		
C294			
L302	L302A		
Y304			
L309	L309A		
G315			
Y316[a]	Y316A, Y316F		
F318	F318A, F318W[c], F318L[c]		F318Y
I319[a]	I319A, I319Y		
C327		C327A	
S330			
H331			
M334	M334E	M334A	
M342			
F345[a]	F345A, F345L		
L347	L347A		
L348			
S359		S359A	
A361	A361L[b], A361 V[b]		
I373			
A375[a]	A375L, A 375 V		
Q377	Q377A		Q377L[b]

[a] Fingerprint residues identified by experimental mutagenesis.[17] [b] Results from ref 63. [c] Results from ref 64. [d] Residues in the 5 Å shell from the TCDD of the selected mAhR model (mAhR_HM01+TCDD) are listed. All mutant AhR analysis results, except those indicated with a reference number, were from the studies described here or our previously mutational analysis.[14,17]

enough to clearly differentiate the higher intermolecular stabilization of THS-017 with respect to THS-020 in the binding site.

Extensive experimental mutagenesis of the mAhR LBD has been carried out over the past few years in order to identify and characterize the key residues involved in TCDD binding, and these experimental data were used to assess the binding pose of TCDD obtained by molecular docking. We focused our attention specifically on the residues contained within the 5 Å shell around the docked ligand (Table 6), and indeed we found that these include all the residues previously identified as the TCDD binding-fingerprint (Figure 4b), for which mutagenesis resulted in the complete loss of TCDD binding and TCDD-induced DNA binding.[17] Other interesting residues that lie within the 5 Å shell around the docked TCDD were identified by site-directed mutagenesis and functional analysis, carried out by our group and others, as important for TCDD binding. In particular: mutation of the residues Pro 291, Phe 318, and Ala 361 reduced or eliminated TCDD binding;[17,63,64] mutation of Cys 327 to Ala partially reduced TCDD binding;[17] Met 334 and Gln 377 mutagenesis had variable effects, with Q377L[63] and M334A[17] having slightly or partially reduced TCDD binding, Q377A with a significantly greater reduction in binding, and M334E with no ligand binding.[17] Mutagenesis of Phe 281 did not appear to affect TCDD binding.[63]

Analysis of the new mAhR LBD homology model and of the TCDD docking also identified other interesting residues that have not been previously examined by mutagenesis and functional analysis (Table 6). Several of these residues (Leu 302, Leu 309, Leu 347, and Ser 359) were selected for experimental mutagenesis analysis as they project their side chains toward the two sides of the elongated binding cavity, with the three leucine residues lining the inner cavity and Ser 359 present at the entrance of the cavity. Accordingly, we generated a series of mutant AhRs containing individual alanine substitutions at these specific positions (L302A, L309A, L347A, and S359A) and demonstrated that these specific mutations did not negatively affect expression levels of the AhRs as each had levels of the *in vitro* expressed protein similar to that of wtAhR (Figure 6a). All the mutations produced significant effects on TCDD binding: AhRs containing L302A, L309A, or L347A mutations exhibited loss of [^{3}H]TCDD binding or dramatically reduced ligand binding activity (to less than 50% of the wtAhR), and ligand binding to the AhR containing the S359A substitution was reduced by ∼40% (Figure 6b). Interestingly, overall reductions in the amount of TCDD-inducible AhR DNA binding observed with each mutant AhR were very similar to the percent loss of ligand binding observed with each (compare Figure 6b and 6c). These results strongly suggest that the loss of ligand-dependent transformation and DNA binding is due to loss of ligand binding activity and is not due to alterations in other steps in ligand-dependent AhR transformation (i.e., hsp90 interactions, ARNT dimerization and/or DNA binding). Therefore, these new mutagenesis data further confirm the proposed binding mode of TCDD in the mAhR binding site, particularly highlighting the role of the hydrophobic environment conferred by the three leucine residues in the inner part of the cavity in ligand stabilization.

Further validation of the reliability of the proposed approach was obtained by docking TCDD into the human AhR model. We previously highlighted[14,65] the critical role of the unique internal residue of huAhR different from a residue of the mAhR, V381 instead of A375 in mAhR (Figure SI1), in determining the lower TCDD binding affinity observed for the huAhR.[33] We proposed that the bigger valine side chain reduces the internal space required for accommodating the TCDD molecule and confirmed this hypothesis by observing the dramatically reduced TCDD binding to the A375 V mutant mAhR.[14,65] These findings were also confirmed by molecular docking, carried out by our group and others, into the homology model of this mutant[17,18] and of the huAhR.[18]

The huAhR homology model was built using the three *holo* HIF-2α structures as templates (alignment in Figure SI1), and four representative conformations were selected from the 100 models generated by MODELLER (selection funnel reported in Scheme 1). The same ensemble docking and minimization procedure adopted for predicting the TCDD binding pose in the mAhR was used (see Experimental Section). The comparison between the Glide XP best scoring pose of TCDD in the huAhR and in the mAhR shows that, even though the modeled cavity volumes were similar (803 Å^3 in huAhR and 813 Å^3 in mAhR), there are differences in the ligand orientation. In particular, the molecular plane of the TCDD is slightly rotated and shifted

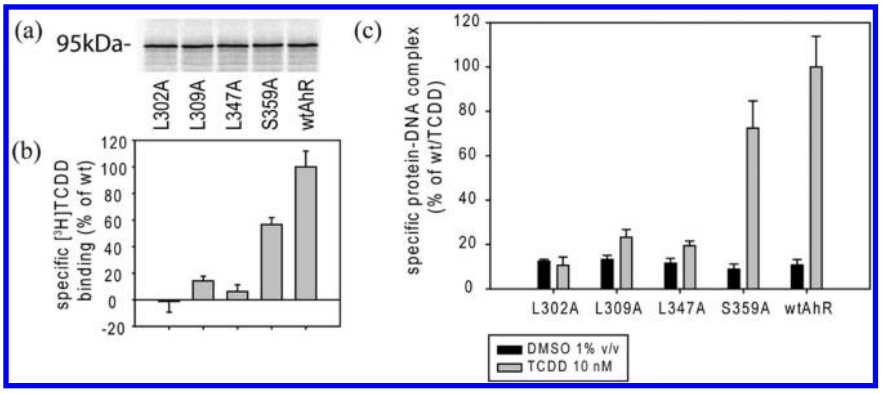

Figure 6. Effect of mutation of key residues in the mAhR ligand binding site and TCDD ligand binding and ligand-dependent DNA binding. (a) Relative expression levels of *in vitro* synthesized wt and mutant AhRs, (b) ligand binding, and (c) DNA binding. (b), (c): Results are presented as the means ± standard deviations of three independent reactions, and results are representative of two independent experiments.

toward the entrance of the cavity in the huAhR, compared to that in the mAhR, and this shift is due to the sterical hindrance of the Val 381 side chain of the huAhR (results not shown). As a consequence, in the huAhR there are increased distances from the ligand to the side chains for which highly stabilizing interactions were predicted from the TCDD/mAhR pose (in particular Gln 383 and Thr 289, corresponding to Gln 377 and Thr 283 in mAhR). Accordingly, the best Glide XP score for the huAhR pose (−7.48) was higher (less favorable) than for the mAhR one (−8.70, in Table 5). Together, these results confirmed the ability of the proposed modeling-docking protocol to correctly rationalize the binding affinity differences for the same ligand within the LBD of the AhRs from different species.

Virtual Ligand Screening of PCDDs. To verify the improvement resulting from the use of AhR LBD models derived from *holo* HIF-2α template structures in ligand docking, as well as to validate the proposed docking protocol, the virtual screening of a set of ligands with known experimental binding affinity data was performed. PCDDs were selected as the ligands for these studies, as they are a class of environmental contaminants that are known to bind to the AhR with a wide range of affinities, from the highest known affinity ligand 2,3,7,8-TCDD to inactive compounds, depending on the chlorine substitution pattern on the aromatic rings.[5−7] In particular, a group of 14 PCDDs for which a homogeneous set of binding affinity data for the rat AhR is available[34,35] were selected for these studies.

Given that the best available set of ligand binding data was derived using rtAhR, a rtAhR LBD homology model was developed using the same protocol described for the mAhR and the huAhR models (the reference sequence alignment is reported in Figure SI1). Four representative models were selected and used for the ensemble docking of PCDDs and the following refinement and rescoring steps (see the Experimental Section). Moreover, the same procedure was also used to analyze PCDD binding to the rtAhR model we developed starting from the *apo* NMR structures of the HIF-2α and ARNT PAS B,[15,16] for comparative purposes.

Similarly to the differences observed in the cavity space of the mAhR *apo* and *holo* models (Table 3), the obtained rtAhR binding cavities also have very different CASTp volumes, ranging from 344 Å^3 to 773 Å^3 for the four representative *apo* models and from 636 Å^3 to 1071 Å^3 for the four representative *holo* models. The Glide XP best scoring poses obtained at the end of the docking, minimization, and rescoring procedure for the 14 PCDDs into the *apo* and *holo* models of the rtAhR are shown in Figure SI4. It can be observed that in the *apo* model (Figure SI4 a) favorable poses into the binding cavity were only found for a limited number of ligands, whereas others were excluded, irrespective of their experimentally established binding affinity. In particular, the poses of the lowest chlorinated PCDDs (1-MCDD and 2,8-DCDD) were predicted in the center of the cavity, while those of six other PCDDs (1,2,3,7,8-PeCDD, 1,3,7,8-TCDD, 2,3,6-TrCDD, 2,3,6,7-TCDD, 2,3,7-TrCDD, and 2,3,7,8-TCDD) were placed at one side of the cavity. The hierarchical series of filters used by the Glide program[57,58,66] to search for possible locations of the ligand excluded the other PCDDs from the binding site, probably due to their sterical hindrance. This group includes OCDD and all the PCDDs that have a bulky substituted aromatic ring due to chlorination at both ortho positions relative to the oxygen atoms (1,2,3,4-TCDD, 1,2,3,4,7-PeCDD, 1,2,3,4,7,8-HxCDD, 1,2,4-TrCDD, 1,2,4,7,8-PeCDD).

In contrast, binding poses were found in the cavity of the *holo* model for all the PCDDs, except OCDD (Figure SI4 b). As expected from the observation that the rtAhR and mAhR modeled binding cavities have similar volumes and share the same internal residues,[17] the predicted 2,3,7,8-TCDD pose lies in the same central region as in the mAhR model and interacts with the same surrounding residues, whose role in TCDD binding to the mAhR was validated by mutagenesis analysis. The other PCDDs were docked in the same zone but with different orientations of the molecular planes and intermolecular interactions; in particular, the poses of the PCDDs that were excluded from the cavity of the *apo* model were placed with the bulky aromatic ring close to the large entrance of the *holo* cavity. It is conceivable that the successful results reported in docking of ligands into the reduced cavity of AhR models derived from the HIF-2α *apo* structure[18,21] is due to the use of different docking protocols having more tolerant intermolecular potentials or explicit treatment of the receptor flexibility.

It is known that docking scoring functions suffer limitations in predicting the binding energies,[59] and a rescoring procedure is often required to obtain a better ranking of the binding poses. Indeed, the Glide XP scoring function was not able to correctly evaluate the observed differences in the PCDD poses in the *holo* rtAhR model and failed to reproduce the experimentally determined ranking of their binding affinities. Therefore, a rescoring of the obtained poses was performed with the molecular mechanics

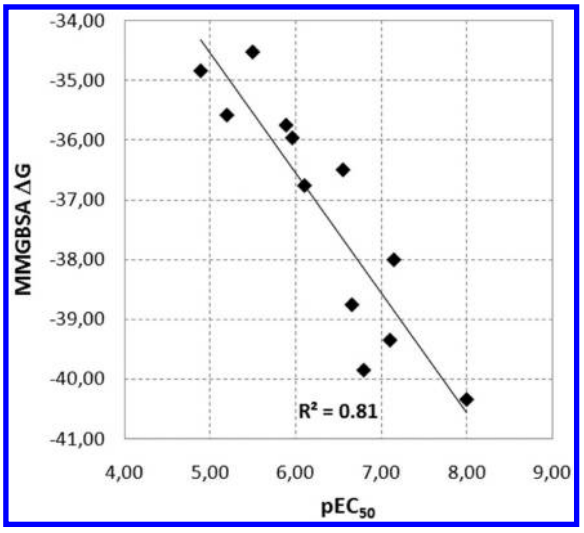

Figure 7. Plot of the calculated $\Delta G_{binding}$ (MM-GBSA) for the docking poses of the 14 PCDDs into the *holo* rtAhR homology model versus their experimental pEC_{50} values for the receptor binding.[34,35]

generalized Born/surface area (MM-GBSA) protocol[67] (see the Experimental Section). Such calculations are largely used in lead optimization for rescoring poses unfavorably ranked by docking programs,[21,68,69] and this method has been proven to perform best for congeneric series of ligands.[21]

The resulting correlation between the MM-GBSA binding free energy and the experimental pEC_{50} values[34,35] for the PCDD set (Figure 7) was very good, with a correlation coefficient $R^2 = 0.81$. Lower correlations with the experimental binding affinities were obtained by other authors, by using similar docking and rescoring programs, for the docking of PCDDs and other classical AhR ligands to an AhR LBD model derived from the *apo* HIF-2α template.[21]

CONCLUSIONS

While an accurate structural description of the ligand binding domain of the AhR would contribute to our understanding of key questions related to ligand binding and ligand-dependent AhR activation, no experimentally determined structures are currently available. Moreover, since all previous homology models of the AhR LBD were derived from *apo* template structures,[13,14,17−21] it is expected that the description of the binding site they provide has some limitations in ligand binding prediction based on molecular docking approaches,[26] particularly for virtual screening applications for which incorporating protein flexibility is computationally too expensive. However, the recent determination of *holo* X-ray structures of the template HIF-2α PAS B domain complexed with several synthetic THS ligands,[30,31] gave us an opportunity to develop a new homology model of the AhR LBD specifically aimed at improving docking reliability.

The AhR functional analysis experiments reported here not only confirmed the ability of two HIF-2α crystallographic ligands to bind to the mAhR with relatively high affinity but also demonstrated that THS-017 and THS-020 were AhR agonists. Together, these results justify the use of the *holo* HIF-2α structures as templates. Indeed, comparative analysis of the *holo* mAhR homology model obtained in this work with the *apo* model developed previously[14] confirmed a significant ligand induced-fit effect that produces a considerable enlargement of the binding cavity. Moreover, the putative binding modes of the THS ligands within the mAhR LBD, evaluated by energy minimization of the mAhR/THS complexes derived from the *holo* model, resulted in good agreement with the mAhR binding site properties.

On the basis of these positive results a specific approach was developed for ligand docking using the new mAhR homology model. It includes ensemble docking to take into account the conformational flexibility of the binding domain and a refinement step consisting of post-docking energy minimization of the obtained complexes. This approach was applied for docking both the THS ligands and TCDD and a good coherence between the virtual ranking of the complexes, obtained by the Glide XP score, and the experimental ranking based on measured ligand binding affinities was obtained. Moreover the obtained TCDD docking poses were consistent with the mutagenesis and mAhR functional analysis data previously generated by our group and others.[14,17,63,64] Additional mutagenesis analyses were based on TCDD docking poses in the new homology model, and the results further confirmed the binding mode obtained for TCDD. Further validation of the proposed approach was obtained from TCDD docking poses into the mAhR and the huAhR that correctly reproduced the experimental evidence for different ligand affinities. Finally, a very satisfactory correlation was obtained between the pEC_{50} values for a set of 14 PCDDs for the rtAhR and the binding free energy of their docking poses, as determined by the MM-GBSA rescoring protocol.

Overall, the agreement between the modeling and experimental results obtained in these studies supports the use of the proposed computational workflow for molecular docking into the new AhR homology model to predict and study the binding modes of structurally diverse ligands in the AhR LBD. This protocol can also be automated by setting up an operative pipeline with KNIME[70] program, in order to perform virtual screening of large collections of compounds.

EXPERIMENTAL SECTION

Expression Plasmids, Site-Directed Mutagenesis, and *in Vitro* Protein Expression. C57BL AhR-expressing plasmid βAhR/pcDNA3 and ARNT-expressing plasmid βARNT/pcDNA3 have been previously described.[12,37,71] AhR point mutants were generated using the QuikChange Multi Lightning site-directed mutagenesis kit (Promega) and mutations verified by sequencing. Wild-type and mutant AhRs and ARNT were synthesized *in vitro* in the presence of L-[^{35}S]methionine (Perkin-Elmer) or unlabeled L-methionine using the TNT Quick coupled transcription/translation rabbit reticulocyte lysate kit (Promega) as previously described.[12]

Ligand Binding Analysis. [^{3}H]TCDD (13 Ci/mmole) was obtained from Dr. Safe (Texas A&M University). [^{3}H]TCDD specific binding and competitive binding analysis for determination of relative ligand binding affinity was carried out using the hydroxyapatite binding assay as previously described for *in vitro* synthesized AhR.[12] The relative binding affinity of THS-017 and THS-022 for the AhR (i.e., IC_{50}s) was determined from nonlinear regression analysis (Sigma Plot) of the competitive binding curves. Expression levels of the *in vitro* synthesized wt and mutant AhR were determined by synthesizing them as ^{35}S-labeled proteins and resolving the denatured proteins by SDS-polyacrylamide gel electrophoresis as described.[14]

Gel Retardation Analysis. Annealed double-stranded oligonucleotides containing the AhR:ARNT DNA binding site (Dioxin

Resposive Element 3, DRE3) from the murine *CYP1A1* upstream regulatory sequence were ^{32}P-labeled and utilized for gel retardation analysis as previously described[12,17,36] with the following changes. *In vitro* synthesized wild-type and mutant mAhR and mARNT reactions were incubated in the absence or presence of 10 nM TCDD for 2 h at room temperature, and an aliquot of the reaction was mixed with buffer containing poly dI•dC (final buffer concentrations were as follows: 25 mM Hepes, pH 7.5, 5 mM ethylenediaminetetraacetic acid, 5 mM dithiotreitol, 10% [v/v] glycerol, 200 mM KCl and 121.9 ng dI•dC) and incubated for 15 min at room temperature followed by addition of ^{32}P-labeled DRE-containing DNA and further incubation at room temperature. TCDD:AhR:ARNT:DRE complexes were resolved by gel retardation analysis as previously described[14,17] and quantitated using a Fujifilm FLA9000 imaging system and MultiGauge software (Fujifilm).

Transient Transfection. COS-1 cells were obtained from the American Type Culture Collection (Manassas, VA) and were maintained in minimum essential medium (αMEM) (Invitrogen) under 5% CO_2 at 37 °C. Transient transfections were performed using lipofectamine 2000 (Invitrogen), with 0.8 μg DNA and 2 μL lipofectamine 2000 added to each well in 24 well plates. Cells were transfected with the following plasmids, per well: 40 ng βAhR/pcDNA3, 200 ng pGudLuc6.1,[39] 40 ng pRL-TK (Promega), and 520 ng of pcDNA3.1+ (Invitrogen) as carrier DNA. After 24 h, cells were incubated for 24 h with indicated concentrations of TCDD (obtained from Dr. S. Safe), and 3-methylcholanthrene (3MC; Sigma-Aldrich), indirubin (AmplaChem, Inc.), alpha-naphthoflavone (aNF; Sigma-Aldrich), or indicated THS compounds. Cells were lyzed and dual luciferase activity measured using the Dual reporter system (Promega) and Orion 1 luminometer (Berthold).

Templates Preparation. X-ray complexes 3F1O, 3H7W, and 3H82 were downloaded by the Protein Data Bank.[72] Chain A, including the HIF-2α/THS ligand complex, has been isolated removing chain B (ARNT protein) and all the crystallographic water molecules.

Protein Preparation Wizard included in Maestro 9v0[73] was used to check structural defects of the raw structural data and to adjust them. The preprocessing step was carried out using all the default values. THS ligands connectivity was corrected as it was improper. The hydrogen bond optimization step was carried out in exhaustive way, and the "Impref optimization" was performed only on the hydrogen with OPLS2005 force field and converging to a rmsd of 0.30 Å.

The corrected and refined HIF-2α/THS ligand structures have then been used for all the subsequent modeling activities.

Homology Modeling. MODELLER version 9v7[42−45] was used to predict mAhR three-dimensional structure. One hundred individual models were obtained by random generation of the starting structure. The "copy ligand" option was activated in order to transfer all the THS ligands from the templates to the final homology models. DOPE scoring[46] was selected to perform the models ranking.

The quality of the obtained models was assessed by the PROCHECK program,[47] that provides information about the stereochemical quality, and by the ProSA validation method,[48,49] that evaluates model accuracy and statistical significance with a knowledge-based potential.

THS Ligands Conformational Search in the Free State. Conformational search of the THS ligands in the free state has been performed using the MacroModel[74] program included in Maestro 9v0[73] with the following parameters: Amber* force field,[75] implicit (Generalized Born/Solvent Accessible, GB/SA) water solvation,[76] automatic set up of the conformational freedom degrees, Monte Carlo Multiple Minimum (MC/MM) random search algorithm with 1000 MC steps for each ligand torsion and Truncated Newton Conjugate Gradient (TNCG) minimization algorithm[77] with a maximum number of iterations of 1500, convergence on a gradient threshold of 0.05 kJ*mol^{-1}*Å^{-1}.

Molecular Mechanics Energy Minimization of the Complexes. Energy minimization of the complexes was carried out using the MacroModel[74] program included in Maestro 9v0[73] with the following parameters: Amber* force field,[75] implicit (Generalized Born/Solvent Accessible, GB/SA) water solvation,[76] Truncated Newton Conjugate Gradient (TNCG) minimization algorithm[77] with a maximum number of iterations of 1500, convergence on a gradient threshold of 0.05 kJ*mol^{-1}*Å^{-1}.

A substructure defining different degrees of system flexibility was prepared for mAhR/THS ligands complexes. THS ligands and the side chains of the residues shell within 5 Å from the THS ligands were defined as free to move; the backbones of the residues shell within 5 Å from the THS ligands were constrained with a force constant of 200 kJ*mol^{-1}*Å^{-2}; the residues within 5−7 Å from the THS ligands were constrained with a force constant of 500 kJ*mol^{-1}*Å^{-2}, and, finally, all the remaining residues were frozen.

For mAhR/TCDD a slightly different substructure was defined to include in the flexible shell also the fingerprint residues previously identified.[17] The TCDD structure, the side chains of the residues shell within 5 Å from the ligand, and the side chains of the fingerprint residues (Thr 283, His 285, Phe 289, Tyr 316, Ile 319, Phe 345, Ala 375) were defined as free to move; the backbone of the residues shell within 5 Å from the ligand and the backbone of the fingerprint residues were constrained with a force constant of 200 kJ*mol^{-1}*Å^{-2}; the residues within 5−7 Å from the ligand were constrained with a force constant of 500 kJ*mol^{-1}*Å^{-2}, and, finally, all the remaining residues were frozen.

Molecular Docking. Molecular docking was carried out using the Glide program[57,58,66] included in Maestro 9v0.[73] Glide uses a hierarchical series of filters to search for possible locations of the ligand in the active-site region of the receptor. The shape and properties of the receptor are represented on a grid by several different sets of fields that provide progressively more accurate scoring of the ligand poses. Ligand conformational flexibility is handled in Glide by an extensive conformational search, augmented by a heuristic screen that rapidly eliminates unsuitable conformations. The final scoring of the poses is carried out using Schrödinger's proprietary GlideScore multiligand scoring function.

Grids for mAhR homology models were set up using default parameters. The binding box was centered in the averaged X, Y, Z coordinates of the three THS ligands centroids with 12 Å sides length. Flexible ligand docking was carried out in standard precision (SP) approach saving only one final pose. All the other parameters are the default ones.

The rescoring of the energy minimized complexes was performed using Glide extra precision (XP) scoring function.[53] All the other parameters are the default ones.

The rescoring of the PCDD docking poses into the rtAhR model was performed by molecular mechanics generalized Born/surface area (MM-GBSA), which uses MD simulations of the free ligand, free protein, and their complex as a basis for calculating

the binding free energy of protein−ligand complexes. This calculation was performed using Prime MM-GBSA,[67] excluding entropic terms, with a flexible receptor shell within 8 Å from the ligand.

Molecular Dynamic Simulations. Monte Carlo/Stochastic Dynamics (MC/SD)[60] performs constant temperature calculations that take advantage of the strengths of Monte Carlo methods for quickly introducing large changes in a few degrees of freedom, and stochastic dynamics for its effective local sampling of collective motions. For MC/SD simulations torsions to be rotated and, if there is more than one molecule in the system, molecules to be translated and rotated must be specified.

MC/SD calculations were carried out using the MacroModel[74] program included in Maestro 9v0.[73] MC/SD workflow starts with an initial energy minimization of the complex that was carried out with the following parameters: Amber* force field,[75] implicit (Generalized Born/Solvent Accessible, GB/SA) water solvation,[76] Truncated Newton Conjugate Gradient (TNCG)[77] minimization algorithm with a maximum number of iterations of 1500, convergence on a gradient threshold of 0.05 kJ*mol^{-1}*Å^{-1}.

Stochastic dynamics was performed with the following parameters: Amber* force field,[75] implicit (Generalized Born/Solvent Accessible, GB/SA) water solvation,[76] no shake, simulation temperature 300 K, time step 1.5 fs, equilibration time 10 ps, simulation time 1500 ps, 1000 structure sampled. The snapshot structures sampled during the simulation were not energy minimized.

TCDD is a rigid molecule, and thus no torsions were varied during the Monte Carlo step that was used to allow its translation (0−5 Å range) and rotation (0°−180° range). The ratio of SD to MC steps was set to 1.

A substructure defining different degrees of system flexibility was prepared and applied in all the steps of the MC/SD: TCDD, the side chains of the residues shell within 5 Å from the ligand and the side chains of the fingerprint residues[17] Thr 283, His 285, Phe 289, Tyr 316, Ile 319, Phe 345, Ala 375 were defined as free to move; the backbones of the residues shell within 5 Å from the ligand and the backbones of the fingerprint residues were constrained with a force constant of 200 kJ*mol^{-1}*Å^{-2}; the residues within 5−7 Å from the ligand were constrained with a force constant of 500 kJ*mol^{-1}*Å^{-2}, and, finally, all the remaining residues were frozen.

■ ASSOCIATED CONTENT

Supporting Information. Figure SI1. Alignment of the LBD domains of mouse, human and rat AhRs against HIF-2α. Figure SI2. Cα-trace representation of the 100 mAhR homology models generated by MODELLER. Figure SI3. Results of ensemble docking of THS-017 and THS-020 in the mAhR homology models. Figure SI4. Results of PCDD ensemble docking in the rtAhR LBD homology models. This material is available free of charge via the Internet at http://pubs.acs.org.

■ AUTHOR INFORMATION

Corresponding Author

*Phone: (+39)0264482821. Fax: (+39)0264482839. E-mail: laura.bonati@unimib.it.

■ ACKNOWLEDGMENT

We thank Dr. Kevin H. Gardner (University of Texas Southwestern) for providing us with the THS ligands and Dr. Steven Safe (Texas A&M University) for TCDD and [^{3}H]TCDD. This work was supported by the National Institutes of Environmental Health Sciences (ES007685 and Superfund Research Grant ES004699) and the California Agricultural Experiment Station.

■ ABBREVIATIONS:

AhR, aryl hydrocarbon receptor; mAhR, *Mus musculus* (mouse) aryl hydrocarbon receptor; huAhR, *Homo sapiens* (human) aryl hydrocarbon receptor; rtAhR, *Rattus norvegicus* (rat) aryl hydrocarbon receptor; ARNT, aryl hydrocarbon receptor nuclear translocator; HIF-2α, hypoxia-inducible factor 2α; hsp90, heat shock protein 90; bHLH, basic helix−loop−helix; DRE, dioxin responsive element; LBD, ligand binding domain; PAS, Per-ARNT-Sim; TCDD, 2,3,7,8-tetrachlorodibenzo-p-dioxin; HAH, halogenated aromatic hydrocarbons; PCDD, polychlorodibenzo-p-dioxins (MCDD, monochloro DCDD, dichloro; TrCDD, trichloro; TCDD, tetrachloro; PeCDD, pentachloro; Hx, hexachloro; O, octhachloro); PCDF, polychlorodibenzofuran; PCB, polychlorobiphenyl; PAH, polycyclic aromatic hydrocarbons; PDB, Protein Data Bank; NMR, nuclear magnetic resonance; rmsd, root-mean-square deviation; HM, homology model; 3MC, 3-methylcholantrene; aNF, alpha-naphthoflavone; DMSO, dimethyl sulfoxide.

■ REFERENCES

(1) Schmidt, J. V.; Bradfield, C. A. Ah receptor signaling pathways. *Annu. Rev. Cell Dev. Biol.* **1996**, *12*, 55–89.

(2) Denison, M. S.; Elferink, C. F.; Phelan, D. The Ah receptor signal transduction pathway. In *Toxicant-Receptor Interactions in the Modulation of Signal Transduction and Gene Expression*; Denison, M. S., Helferich, W. G., Eds.; Taylor and Francis: Bristol, PA, 1998; pp 3−33.

(3) Ma, Q. Induction of CYP1A1. The AhR/DRE paradigm: Transcription, receptor regulation, and expanding biological roles. *Curr. Drug Metab.* **2001**, *2*, 149–164.

(4) Kewley, R. J.; Whitelaw, M. L.; Chapman-Smith, A. The mammalian basic helix-loop-helix/PAS family of transcriptional regulators. *Int. J. Biochem. Cell Biol.* **2004**, *36*, 189–204.

(5) Poland, A.; Knutson, J. C. 2,3,7,8-Tetrachlorodibenzo-p-dioxin and related halogenated aromatic hydrocarbons: examination of the mechanism of toxicity. *Annu. Rev. Pharmacol. Toxicol.* **1982**, *22*, 517–542.

(6) Safe, S. Polychlorinated biphenyls (PCBs), dibenzo-p-dioxins (PCDDs), dibenzofurans (PCDFs), and related compounds: environmental and mechanistic considerations which support the development of toxic equivalency factors (TEFs). *Crit. Rev. Toxicol.* **1990**, *21*, 51–88.

(7) Denison, M. S.; Seidel, S. D.; Rogers, W. J.; Ziccardi, M.; Winter, G. M.; Heath-Pagliuso, S. Natural and synthetic ligands for the Ah receptor. In *Molecular Biology Approaches to Toxicology*; Puga, A., Wallace, K. B., Eds.; Taylor & Francis: Philadelphia, PA, 1998; pp 393−410.

(8) Denison, M. S.; Heath-Pagliuso, S. The Ah receptor: A regulator of the biochemical and toxicological actions of structurally diverse chemicals. *Bull. Environ. Contam. Toxicol.* **1998**, *61*, 557–568.

(9) Denison, M. S.; Pandini, A.; Nagy, S. R.; Baldwin, E. P.; Bonati, L. Ligand binding and activation of the Ah receptor. *Chem. Biol. Interact.* **2002**, *141*, 3–24.

(10) Denison, M. S.; Nagy, S. R. Activation of the aryl hydrocarbon receptor by structurally diverse exogenous and endogenous chemicals. *Annu. Rev. Pharmacol. Toxicol.* **2003**, *43*, 309–334.

(11) Nguyen, L. P.; Bradfield, C. A. The search for endogenous activators of the aryl hydrocarbon receptor. *Chem. Res. Toxicol.* **2008**, *21*, 102–106.

(12) Soshilov, A. A.; Denison, M. S. Role of the Per/Arnt/Sim domains in ligand-dependent transformation of the aryl hydrocarbon receptor. *J. Biol. Chem.* **2008**, *283*, 32995–32305.

(13) Procopio, M.; Lahm, A.; Tramontano, A.; Bonati, L.; Pitea, D. A model for recognition of polychlorinated dibenzo-p-dioxins by the aryl hydrocarbon receptor. *Eur. J. Biochem.* **2002**, *269*, 13–18.

(14) Pandini, A.; Denison, M. S.; Song, Y.; Soshilov, A. A.; Bonati, L. Structural and functional characterization of the aryl hydrocarbon receptor ligand binding domain by homology modeling and mutational analysis. *Biochemistry* **2007**, *46*, 696–708.

(15) Erbel, P. J.; Card, P. B.; Karakuzu, O.; Bruick, R. K.; Gardner, K. H. Structural basis for PAS domain heterodimerization in the basic helix-loop-helix-PAS transcription factor hypoxia-inducible factor. *Proc. Natl. Acad. Sci. U.S.A.* **2003**, *100*, 15504–15509.

(16) Card, P. B.; Erbel, P. J.; Gardner, K. H. Structural basis of Arnt PAS-B dimerization: use of a common beta-sheet interface for hetero- and homodimerization. *J. Mol. Biol.* **2005**, *353*, 664–678.

(17) Pandini, A.; Soshilov, A. A.; Song, Y.; Zhao, J.; Bonati, L.; Denison, M. S. Detection of the TCDD binding-fingerprint within the Ah receptor ligand binding domain by structurally driven mutagenesis and functional analysis. *Biochemistry* **2009**, *48*, 5972–5983.

(18) Bisson, W. H.; Koch, D. C.; O'Donnell, E. F.; Khalil, S. M.; Kerkvliet, N. I.; Tanguay, R. L.; Abagyan, R.; Kolluri, S. K. Modeling of the aryl hydrocarbon receptor (AhR) ligand binding domain and its utility in virtual ligand screening to predict new AhR ligands. *J. Med. Chem.* **2009**, *52*, 5635–5641.

(19) Wu, B.; Zhang, Y.; Kong, J.; Zhang, X.; Cheng, S. In silico predication of nuclear hormone receptors for organic pollutants by homology modeling and molecular docking. *Toxicol. Lett.* **2009**, *191*, 69–73.

(20) Yoshikawa, E.; Miyagi, S.; Dedachi, K.; Ishihara-Sugano, M.; Itoh, S.; Kurita, N. Specific interactions between aryl hydrocarbon receptor and dioxin congeners: Ab initio fragment molecular orbital calculations. *J. Mol. Graphics Modell.* **2010**, *29*, 197–205.

(21) Jogalekar, A. S.; Reiling, S.; Vaz, R. J. Identification of optimum computational protocols for modeling the aryl hydrocarbon receptor (AhR) and its interaction with ligands. *Bioorg. Med. Chem. Lett.* **2010**, *20*, 6616–9.

(22) Murray, I. A.; Flaveny, C. A.; Chiaro, C. R.; Sharma, A. K.; Tanos, R. S.; Schroeder, J. C.; Amin, S. G.; Bisson, W. H.; Kolluri, S. K.; Perdew, G. H. Suppression of cytokine-mediated complement factor gene expression through selective activation of the Ah receptor with 3′,4′-dimethoxy-α-naphthoflavone. *Mol. Pharmacol.* **2011**, *79*, 508–19.

(23) Hillisch, A.; Pineda, L. F.; Hilgenfeld, R. Utility of homology models in the drug discovery process. *Drug Discovery Today* **2004**, *9*, 659–669.

(24) Ferrara, P.; Jacoby, E. Evaluation of the utility of homology models in high throughput docking. *J. Mol. Model.* **2007**, *8*, 897–905.

(25) Cavasotto, C. N.; Phatak, S. S. Homology modeling in drug discovery: current trends and applications. *Drug Discovery Today* **2009**, *14*, 676–683.

(26) McGovern, S. L.; Shoichet, B. K. Information decay in molecular docking screens against holo, apo, and modeled conformations of enzymes. *J. Med. Chem.* **2003**, *46*, 2895–2907.

(27) Fan, H.; Irwin, J. J.; Webb, B. M.; Klebe, G.; Shoichet, B. K.; Sali, A. Molecular docking screens using comparative models of proteins. *J. Chem. Inf. Model.* **2009**, *49*, 2512–2527.

(28) Bordogna, A.; Pandini, A.; Bonati, L. Predicting the accuracy of protein-ligand docking on homology models. *J. Comput. Chem.* **2011**, *32*, 81–98.

(29) Rockey, W. M.; Elcock, A. H. Structure selection for protein kinase docking and virtual screening: homology models or crystal structures? *Curr Protein Pept. Sci.* **2006**, *7*, 437–457.

(30) Scheuermann, T. H.; Tomchick, D. R.; Machius, M.; Guo, Y.; Bruick, R. K.; Gardner, K. H. Artificial ligand binding within the HIF2α transcription factor. *Proc. Natl. Acad. Sci. U.S.A.* **2009**, *106*, 450–455.

(31) Key, J.; Scheuermann, T. H.; Anderson, P. C.; Daggett, V.; Gardner, K. H. Principles of ligand binding within a completely buried cavity in HIF2α PAS-B. *J. Am. Chem. Soc.* **2009**, *131*, 17647–17654.

(32) Amezcua, C. A.; Harper, S. M.; Rutter, J.; Gardner, K. H. Structure and interactions of PAS kinase N-terminal PAS domain: Model for intramolecular kinase regulation. *Structure* **2002**, *10*, 1349–1361.

(33) Ema, M.; Ohe, N.; Suzuki, M.; Mimura, J.; Sogawa, K.; Ikawan, S.; Fujii-Kuriyama, Y. Dioxin binding activities of polymorphic forms of mouse and human arylhydrocarbon receptors. *J. Biol. Chem.* **1994**, *269*, 27337–27343.

(34) Mason, G.; Farrell, K.; Keys, B.; Piskorska-Pliszczynska, J.; Safe, L.; Safe, S. Polychlorinated dibenzo-p-dioxins: quantitative in vitro and in vivo structure-activity relationships. *Toxicology* **1986**, *41*, 21–31.

(35) Safe, S. H. Comparative toxicology and mechanism of action of polychlorinated dibenzo-p-dioxins and dibenzofurans. *Annu. Rev. Pharmacol. Toxicol.* **1986**, *26*, 371–399.

(36) Denison, M. S.; Rogers, J. M.; Rushing, S. R.; Jones, C. L.; Tetangco, S. C.; Heath-Pagliuso, S. Analysis of the Ah Receptor Signal Transduction Pathway. In *Current Protocols in Toxicology*; Maines, M., Costa, L. G., Reed, D. J. Sassa, S., Sipes, I. G., Eds.; John Wiley and Sons: New York, NY, 2002; pp (4.8)1−(4.8)45.

(37) Poland, A.; Glover, E.; Kende, A. Stereospecific, high affinity binding of 2,3,7,8-tetrachlorodibenzo-p-dioxin by hepatic cytosol. Evidence that the binding species is receptor for induction of aryl hydrocarbon hydroxylase. *J. Biol. Chem.* **1976**, *251*, 4936–4946.

(38) Denison, M. S.; Wilkinson, C. F.; Okey, A. B. Ah receptor for 2,3,7,8-tetrachlorodibenzo-p-dioxin: comparative studies in mammalian and nonmammalian species. *Chemosphere* **1986**, *15*, 1665–1672.

(39) Han, D. H.; Nagy, S. R.; Denison, M. S. Comparison of recombinant cell bioassays for the detection of Ah receptor agonists. *Biofactors* **2004**, *20*, 11–22.

(40) Petkov, P. I.; Rowlands, J. C.; Budinsky, R.; Zhao, B.; Denison, M. S.; Mekenyan, O. Mechanism based common reactivity pattern (COREPA) modeling of AhR binding affinity. *SAR QSAR Environ. Res.* **2010**, *21*, 187–214.

(41) Andersen, C. A.; Palmer, A. G.; Brunak, S.; Rost, B. Continuum secondary structure captures protein flexibility. *Structure* **2002**, *10*, 175–184.

(42) Sali, A.; Blundell, T. L. Comparative protein modeling by satisfaction of spatial restraints. *J. Mol. Biol.* **1993**, *234*, 779–815.

(43) Marti-Renom, M. A.; Stuart, A.; Fiser, A.; Sanchez, R.; Melo, F.; Sali, A. Comparative protein structure modeling of genes and genomes. *Annu. Rev. Biophys. Biomol. Struct.* **2002**, *29*, 291–325.

(44) Fiser, A.; Do, R. K.; Sali, A. Modeling of loops in protein structures. *Protein Sci.* **2000**, *9*, 1753–1773.

(45) Modeller. Program for Comparative Protein Structure Modelling by Satisfaction of Spatial Restraints. http://www.salilab.org/modeller/ (accessed Nov 8, 2010).

(46) Shen, M.; Sali, A. Statistical potential for assessment and prediction of protein structures. *Protein Sci.* **2006**, *15*, 2507–2524.

(47) Laskowski, R. A.; MacArthur, M. W.; Moss, D. S.; Thornton, J. M. PROCHECK: a program to check the stereochemical quality of protein structures. *J. Appl. Crystallogr.* **1993**, *26*, 283–291.

(48) Sippl, M. J. Recognition of errors in three-dimensional structures of proteins. *Proteins* **1993**, *17*, 355–362.

(49) Wiederstein, M.; Sippl, M. J. ProSA-web: Interactive web service for the recognition of errors in three-dimensional structures of proteins. *Nucleic Acids Res.* **2007**, *35*, W407–W410.

(50) Dundas, J.; Ouyang, Z.; Tseng, J.; Binkowski, A.; Turpaz, Y.; Liang, J. CASTp: Computed atlas of surface topography of proteins with structural and topographical mapping of functionally annotated residues. *Nucleic Acids Res.* **2006**, *34*, W116–W118.

(51) CASTp. Computed Atlas of Surface Topography of proteins. http://sts.bioengr.uic.edu/castp/ (accessed Nov 8, 2010).

(52) Connolly, M. L. Analytical molecular surface calculation. *J. Appl. Crystallogr.* **1983**, *16*, 548–558.

(53) Friesner, R. A.; Murphy, R. B.; Repasky, M. P.; Frye, L. L.; Greenwood, J. R.; Halgren, T. A.; Sanschagrin, P. C.; Mainz, D. T. Extra precision Glide: Docking and scoring incorporating a model of hydrophobic enclosure for protein-ligand complexes. *J. Med. Chem.* **2006**, *49*, 6177–6196.

(54) Huang, S. Y.; Zou, X. Advances and challenges in protein-ligand docking. *Int. J. Mol. Sci.* **2010**, *11*, 3016–3034.

(55) B-Rao, C.; Subramanian, J.; Sharma, S. D. Managing protein flexibility in docking and its applications. *Drug Discovery Today* **2009**, *14*, 394–400.
(56) Novoa, E. M.; de Pouplana, L. R.; Barril, X.; Orozco, M. Ensemble docking from homology models. *J. Chem. Theory Comput.* **2010**, *6*, 2547–2557.
(57) Friesner, R. A.; Banks, J. L.; Murphy, R. B.; Halgren, T. A.; Klicic, J. J.; Mainz, D. T.; Repasky, M. P.; Knoll, E. H.; Shaw, D. E.; Shelley, M.; Perry, J. K.; Francis, P.; Shenkin, P. S. Glide: A new approach for rapid, accurate docking and scoring. 1. Method and assessment of docking accuracy. *J. Med. Chem.* **2004**, *47*, 1739–1749.
(58) Halgren, T. A.; Murphy, R. B.; Friesner, R. A.; Beard, H. S.; Frye, L. L.; Pollard, W. T.; Banks, J. L. Glide: A new approach for rapid, accurate docking and scoring. 2. Enrichment factors in database screening. *J. Med. Chem.* **2004**, *47*, 1750–1759.
(59) Warren, G. L.; Andrews, C. W.; Capelli, A. M.; Clarke, B.; LaLonde, J.; Lambert, M. H.; Lindvall, M.; Nevins, N.; Semus, S. F.; Senger, S.; Tedesco, G.; Wall, I. D.; Woolven, J. M.; Peishoff, C. E.; Head, M. S. A critical assessment of docking programs and scoring functions. *J. Med. Chem.* **2006**, *49*, 5912–5931.
(60) Guarnieri, F.; Still, W. C. A rapidly convergent simulation method: Mixed Monte Carlo/Stochastic Dynamics. *J. Comput. Chem.* **1994**, *15*, 1302–1310.
(61) Metropolis, N.; Rosenbluth, A. W.; Rosenbluth, M. N.; Teller, A. H.; Teller, E. Equation of state calculations by fast computing machines. *J. Chem. Phys.* **1953**, *21*, 1087–1093.
(62) *SiteMap*, version 2.3; Schrödinger, LLC: New York, NY, 2009.
(63) Henry, E. C.; Gasiewicz, T. A. Molecular determinants of species-specific agonist and antagonist activity of a substituted flavone towards the aryl hydrocarbon receptor. *Arch. Biochem. Biophys.* **2008**, *472*, 77–88.
(64) Goryo, K.; Suzuki, A.; Del Carpio, C. A.; Siizaki, K.; Kuriyama, E.; Mikami, Y.; Kinoshita, K.; Yasumoto, K.; Rannug, A.; Miyamoto, A.; Fujii-Kuriyama, Y.; Sogawa, K. Identification of amino acid residues in the Ah receptor involved in ligand binding. *Biochem. Biophys. Res. Commun.* **2007**, *354*, 396–402.
(65) Murray, I. A.; Reen, R. K.; Leathery, N.; Ramadoss, P.; Bonati, L.; Gonzalez, F. J.; Peters, J. M.; Perdew, G. H. Evidence that ligand binding is a key determinant of Ah receptor mediated transcriptional activity. *Arch. Biochem. Biophys.* **2005**, *442*, 59–71.
(66) *Glide*, version 5.5; Schrödinger, LLC: New York, NY, 2009.
(67) *Prime*, version 2.2; Schrödinger, LLC: New York, NY, 2010.
(68) Graves, A. P.; Shivakumar, D. M.; Boyce, S. E.; Jacobson, M. P.; Case, D. A.; Shoichet, B. K. Rescoring docking hit lists for model cavity sites: predictions and experimental testing. *J. Mol. Biol.* **2008**, *377*, 914–934.
(69) Guimarães, C. R.; Cardozo, M. MM-GB/SA rescoring of docking poses in structure-based lead optimization. *J. Chem. Inf. Model.* **2008**, *48*, 958–970.
(70) KNIME. http://www.knime.org/ (accessed Mar 14, 2011).
(71) Fukunaga, B. N.; Hankinson, O. Identification of a novel domain in the aryl hydrocarbon receptor required for DNA binding. *J. Biol. Chem.* **1996**, *283*, 3743–3749.
(72) RCSB PDB. http://www.rcsb.org/pdb/home/home.do (accessed Oct 11, 2010).
(73) *Maestro*, version 9.0; Schrödinger, LLC: New York, NY, 2009.
(74) *MacroModel*, version 9.7; Schrödinger, LLC: New York, NY, 2009.
(75) McDonald, D. Q.; Still, W. C. AMBER torsional parameters for the peptide backbone. *Tetrahedron Lett.* **1992**, *33*, 7743–7746.
(76) Still, W. C.; Tempczyk, A.; Hawlely, R. C.; Hendrickson, T. A. General treatment of solvation for molecular mechanics. *J. Am. Chem. Soc.* **1990**, *112*, 6127–6129.
(77) Leach, A. R. *Molecular Modelling: Principles and Applications*, 2nd ed.; Pearson Prentice Hall: Harlow, England, 2001.